27

Egypt. J. Chem. **53**, No. **3** , pp. 417 - 434 (2010)

Synthesis and Structural Characterization of Lithiated and Delithiated $LiCoO_2$ Using Different Chelating Agents

A.E. Abdel-Ghany[#], A.E. Eid, Aida A. Salman[*], Carmen M. Sharaby[*] and Suzan K. Abdel-Hamied

Inorganic Chemistry Department, National Research Center, and [*]Chemistry Department, Faculty of Science, Al-Azhar University(Girls), Cairo, Egypt.

LAYERED $LiCoO_2$ was synthesized by sol-gel method using succinic, malic and tartaric acid as chelating agent. The delithiated Li_xCoO_2 oxide was obtained by chemically extracting lithium from the corresponding $LiCoO_2$ with the oxidizer $K_2S_2O_8$. X-Ray Diffraction (XRD), Scanning Electron Microscope (SEM), Transmission Electronic Microscope (TEM), Fourier Transform Infra-Red (FTIR), and Raman Scattering (RS) were used for characterization of the lithiated and delithiated phase. It shows that the samples obtained are layered $LiCoO_2$ with the α-$NaFeO_2$ structure. All the samples are homogenous and the particle size can be easily controlled by the preparation temperature. Upon lithium deintercalation from the host material, two different phases can be found.

Keywords: Transition-metal oxides, Layered structure, Spinel structure, Intercalation compounds. Cathode materials, Vibration spectroscopy and Li-ion batteries.

The lithium-ion battery was "born" in 1991 and grew rapidly as the power source of choice for portable electronic devices, especially wireless telephones and laptop computers, during the past 20 years. A lot of researches on physical and electrochemical properties of $LiCoO_2$ have been carried out for the applications of high-energy density electric vehicles[(1–5)] . $LiCoO_2$ is one of the most extensively used cathode material in rechargeable lithium ion batteries. It has been used as a cathode material without hesitation since its performance as cathode is excellent and its advantages, such as high operating voltage, high specific capacity and long cycle life are evident. In addition, the size and the shape of the particles used to prepare the electrodes have important influence on the high rate performance of lithium-ion batteries[(6)]. For example, smaller particles provide shorter pathways for solid-state diffusion of Li ions[(7)]. The dependence of electrochemical cyclability of $LiCoO_2$ cathodes on the particle size of cathode material has been reported [(8)].

$LiCoO_2$ crystallizes with the rhombohedral symmetry ($R\bar{3}m$ space group), which is made up of Li and Co cations occupying the octahedral sites of a ccp

[*]Corresponding author: e-mail address: achraf_28@yahoo.com.

array of oxide ions in alternate layers (Fig. 1). Nanocrystalline $LiCoO_2$ synthesized through a posttemplating method [9], a molten salt method [10, 11], a spray-drying method [12], a co-precipitation method [13] and a hydrothermal method[14–17] have been reported. However, these methods require difficult conditions a large quantity of solvent and organic materials [18]. The sol–gel method has been reported to be one of the simplest methods to prepare multi-component oxides [19, 20].

FTIR and RS, which are the most important tools for the investigation of vibrational structures of molecules and a sensitive probe to the local atomic arrangements, have been used to characterize the microstructure of many nanomaterials[21-25]. In this framework, we report in this paper both synthesis and structural properties of $LiCoO_2$ powder in relation to the mode of preparation by wet-chemical method. The vibration spectroscopies were used to investigate the phase change of lithiated and delithiated $LiCoO_2$.

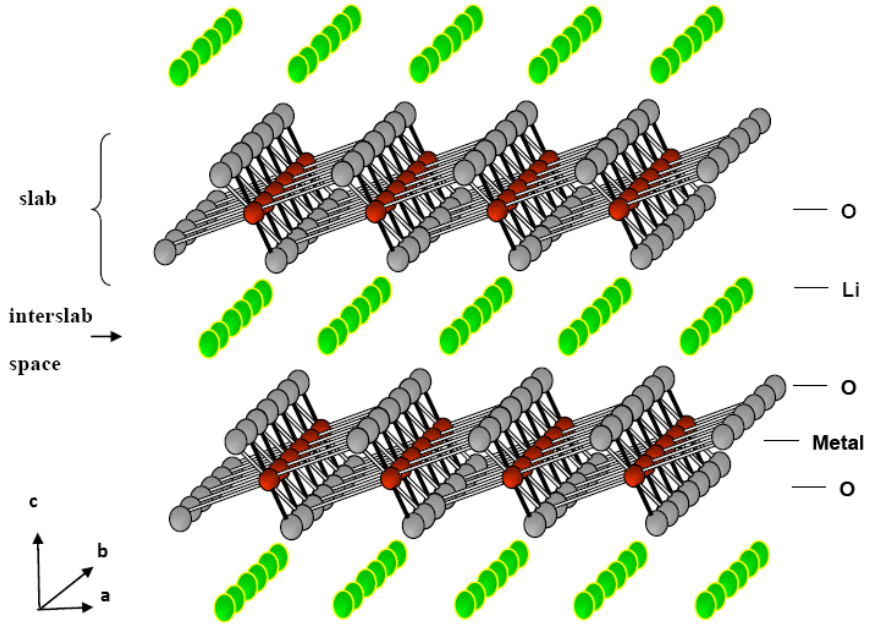

Fig. 1. Schematic representation of the ideal structure of the positive electrode material $Li(M)O_2$ showing the alternating layers formed by edge-sharing $(M)O_6$ octahedra and Li^+ ions.

Experimental

The wet-chemical route assisted by carboxylic acid was used to synthesize $LiCoO_2$ materials. $LiCoO_2$ powders were prepared using appropriate molar ratios of lithium and cobalt acetate. Three samples were synthesized in presence of succinic, malic and tartaric acid, respectively. The dried xerogels were calcined in air at 450°C for 5 hr to convert the metal carboxylates to oxides. The resulting

products were sintered at 800°C in air for 12 hr. The sol–gel and combustion synthesis occurred from metal acetates via inorganic polymerization reactions in solution according to methods reported in our previous work [26]. Compared with the conventional solid state reaction, it is believed that these techniques offer many advantages, such as a lower temperature processing and a better control of material morphology.

The next section shows that among the three samples, the sample that has the best structural properties is the one prepared in presence of malic acid. Therefore, we have chosen that sample to study delithiation effects. The removal of lithium ions from the layered framework has been carried out by an oxidizing agent (potassium peroxydisulfate ($K_2S_2O_8$)) in an aqueous solution. The degree of delithiation was controlled by adjusting the amount of the oxidant. The mixture of $LiCoO_2$ and $K_2S_2O_8$ dissolved in water was stirred at room temperature for 24 hr. Then, the powders were washed, filtered and dried at 200°C.

DTA–TG curves of the gel precursor were obtained using a thermogravimetric analyzer (Perkin Elmer, TGA 7 series) in the temperature range of 30–1000°C in air at a heating rate of 10°C/min. The crystal structure of $LiCoO_2$ samples was analyzed by X-ray diffractometry (XRD) using a Philips X'Pert apparatus equipped with a Cu Kα X-ray source (λ = 1.5406 A°). XRD measurements were collected in the 2θ range 10–80°.The particle morphology of the $LiCoO_2$ powders was examined with a scanning electron microscope (SEM, JEOL-Japan, JXA-840A) and transmission electronic microscope (TEM JEOL-1230). Raman spectra were collected with a Jobin-Yvon U1000 double-pass spectrometer equipped with a cooled, low noise photomultiplier tube (ITT FW130). The incident light used for the experiments was the 515 nm Ar line of a laser source. FTIR spectra were recorded with a Bruker IFS 113 vacuum interferometer. In the far-infrared region (400-100cm^{-1}), the vacuum bench apparatus was equipped with a 3.5μm thick Mylar beam splitter, a globar source and a DTGS/PE far-infrared detector.

Results and Discussion

Synthesis and thermal analysis

Figures 2-4 show the TG and DTA curves of $LiCoO_2$ xerogel synthesized by wet chemistry assisted by three carboxylic acids: succinic, malic, and tartaric acid, respectively. We observed three steps during the course of aqueous solutions heat-treatment. The first step associated with the weak endothermic effect (T<250°C) accompanied with a small weight loss, attributed to departure of residual water. After the departure of the remaining water molecule, a strong exothermic peak appears. This exothermic effect corresponds to the combustion of carboxylic acid and acetate ions xerogel. More than half of the weight loss occurs during this stage due to a violent oxidation decomposition reaction. It appeared that carboxylic acid acts as a fuel in the pyrolysis of the gel precursor,

favoring the decomposition of acetate ions. It was reported that chelating agent (carboxylic-based acid) provokes decomposition during the synthesis of oxide powders [27-29]. The gel precursor was burning because the decomposed acetate ions acted as an oxidizer.

For succinic acid (Fig. 2), the initial weight loss for the water departure is 11.44% while 49.438% weight loss in the temperature range 280-460°C corresponds to the decomposition of the organic constituents. The exothermic effect occurs at ca. 442.5°C. For malic acid (Fig. 3), the initial weight loss for the water departure is 12.89% while 51.53% weight loss occurs in the temperature range 320-360°C. This composition exhibits a strong exothermic peak at 347.7°C. For tartaric acid (Fig. 4), the initial weight loss for the water departure is 13.37% while 45.55% weight loss occurs in the temperature range 300-490°C. This composition exhibits strong exothermic peaks at 444 and 470°C. The last step consists in the production of the mass precursor. Even though the crystallization starts around 450°C for malic and around 550°C for succinic and tartaric acid, the well-crystallized and single phases have been obtained at 600,500 and 600°C for succinic, malic and tartaric acid, respectively. The total weight loss for $(NH_4)_2LiCo(C_4H_4O_5)$ is about 66%, which agrees well with the calculated values for a final product of composition $LiCoO_2$ (63.6%) assisted by malic acid for example. XRD studies after the last effect indicate that very intimately mixed lithium cobalt–oxides reacted together.

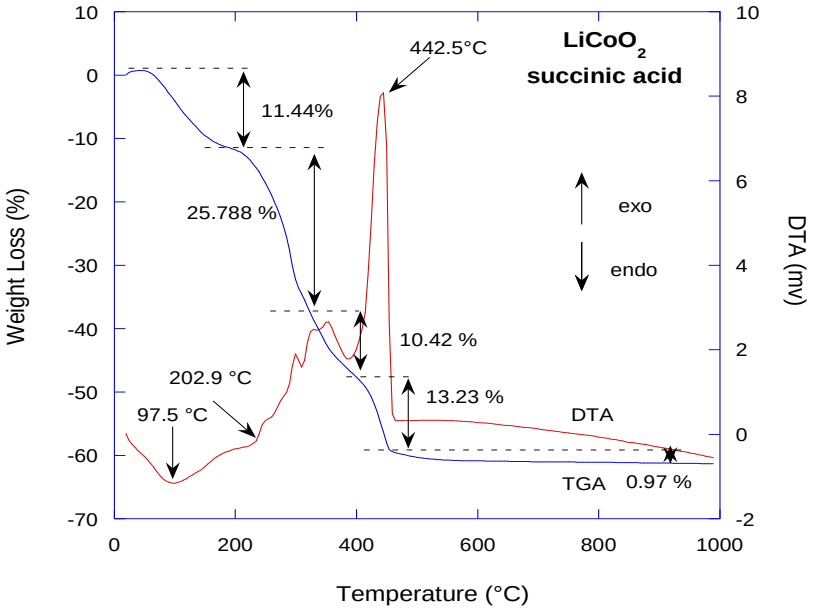

Fig. 2. TG-DTA pattern of $LiCoO_2$ xerogel synthesized by sol –gel technique assisted succinic acid.

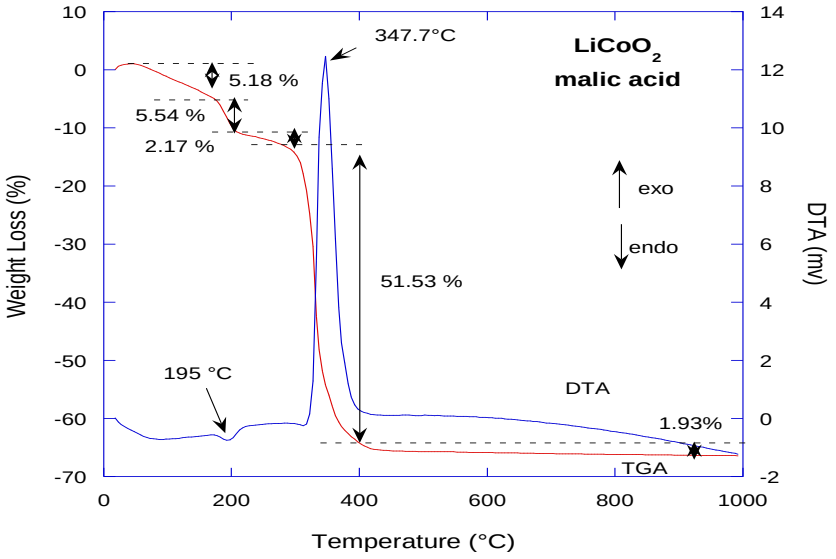

Fig. 3. TG-DTA pattern of $LiCoO_2$ xerogel synthesized by sol –gel technique assisted malic acid.

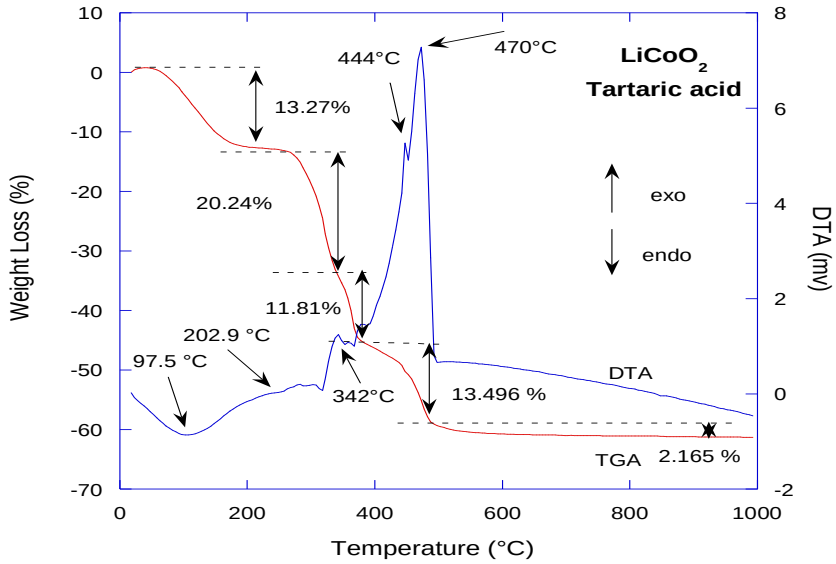

Fig. 4. TG-DTA pattern of $LiCoO_2$ xerogel synthesized by sol –gel technique assisted tartaric acid.

Structure and morphology

Figure 5 shows the XRD patterns of $LiCoO_2$ samples synthesized by wet-chemistry and calcined at 800°C in air for 12 hr. Bragg lines are indexed in the $R\bar{3}m$ space group with the hexagonal sitting. No impurity phases were detected by XRD and the powders were crystallized in the α-$NaFeO_2$-type structure. Table 1 lists the lattice constants for the three samples. The well separated (1 0 8) / (1 1 0) doublet around 2θ =66° and the c_{hex}/a_{hex} ratio indicate the good anisotropy of the layered framework. The XRD pattern of the sample prepared from malate precursor shows the best crystallinity so far. Its more detail XRD pattern is inserted in Fig. 5. The plot of the intensity ratio of XRD lines $I_{0\,0\,3}/I_{1\,0\,4}$ that is known to depend on the degree of displacement between the cations located at 3*a* and 3*b* sites in the $R\bar{3}m$ space group is shown in Fig.6 [30, 31]. The higher the ratio, the less the cationic disorder. On this basis, the degree of cationic disorder is reduced in $LiCoO_2$ for calcination temperature of 800°C. The lattice constant ratio *c*/*a* is also reported in Fig.6 as a function of the calcination temperature for $LiCoO_2$ powders synthesized by wet-chemistry, together with the values reported in prior works [32-35]. There is a wide range for the *c*/*a* ratio depending on the synthesis procedure and the sintering conditions. The general trend for the $LiCoO_2$ lattice makes our sample with c_{hex}/a_{hex} = 4.998 in the range of the characteristic value for α-$NaFeO_2$ layered structure.

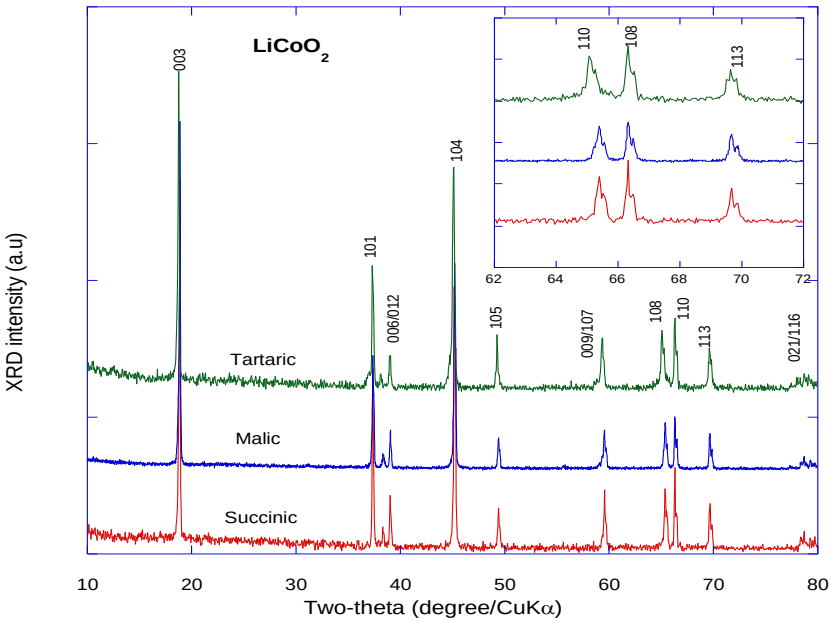

Fig. 5. XRD pattern of $LiCoO_2$ powders synthesized by wet chemistry assisted by three carboxylic acids: succinic, malic, and tartaric. Bragg lines are indexed in the $R\bar{3}m$ space group with the hexagonal sitting. Insert shows detail in the range 2θ=62-72° for the three samples.

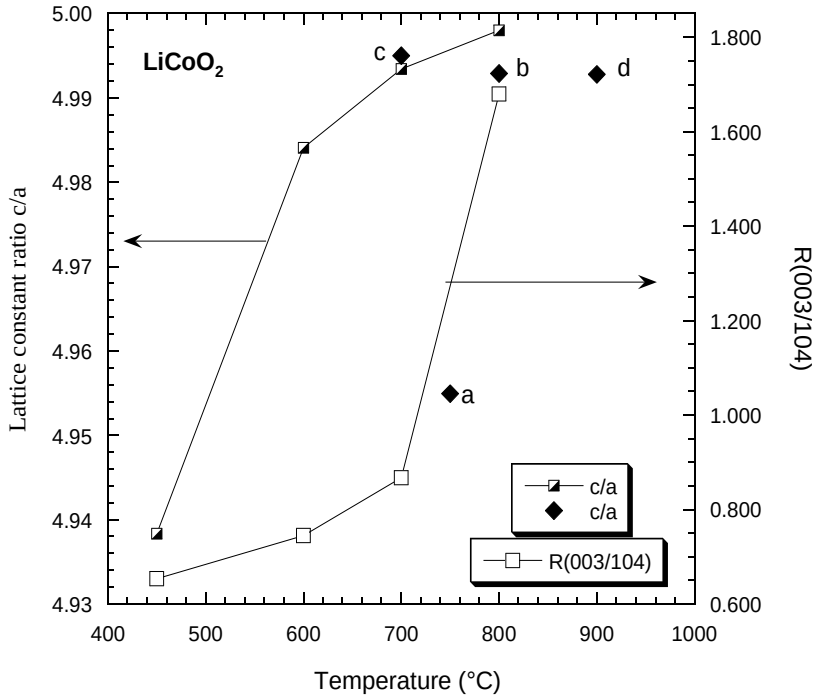

Fig. 6. Plot of the intensity ratio of XRD lines I_{003}/I_{104} and lattice constant ratio c/a as a function of the calcinations temperature for $LiCoO_2$ powders synthesized by wet chemistry. Diamonds represent the literature data from (a) Castro-Garcia *et al*. [32], (b) Lee *et al*. [33], (c) Vivekanandhan *et al*. [34], and (d) Clémencon *et al*. [35].

TABLE.1. XRD data obtained on $LiCoO_2$ powders calcined at 800°C, prepared by wet-chemistry method assisted by succinic, malic and tartaric acid as chelating agents.

$LiCoO_2$	a_{hex}(Å)	c_{hex} (Å)	c_{hex}/a_{hex}	Unit-cell volume (Å^3)	I_{003}/I_{104}	δ *nm*
Succinic acid	2.81(6)	14.07(6)	4.99(8)	96.66	1.41	42
Malic acid	2.81(5)	14.06(8)	4.99(8)	96.54	1.68	40
Tartaric acid	2.81(5)	14.07(6)	4.99(2)	96.55	1.45	70

The morphology of powders calcined in the range 600–800°C has been determined by SEM and TEM. Figure 7a-c shows the SEM micrographs of $LiCoO_2$ powders prepared from the wet-chemical method assisted by malic acid for material fired at 600,700 and 800°C in air for 12hr, while Fig.7d shows the TEM micrographs of $LiCoO_2$ powders prepared from the wet-chemical method assisted by malic acid for material fired at 800°C. Obviously, the modification in the particle morphology occurred upon sustained calcination process. It is worth noting that the low-temperature synthesis provides sub-micron size particles with a fairly narrow distribution. The SEM and TEM pictures reveal that in both

cases, the products contain 30–100nm particles corresponding well to the 40 nm average particle size calculated from XRD data by the Scherrer's formula.

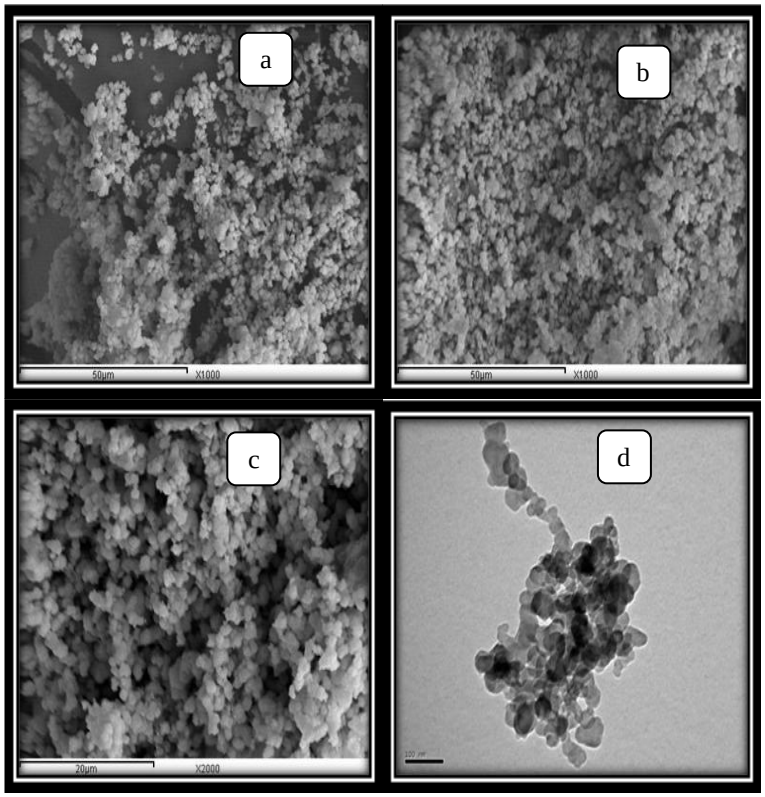

Fig. 7. SEM morphologies of the $LiCoO_2$ samples synthesized by wet-chemistry method assisted by malic acids at different temperatures: (a) 600°C, (b) 700°C, (c) 800°C, and (d) TEM at 800°C for 12hr.

Vibration spectroscopy

Local structure, nanodomain formation, and change in cation ordering have been observed by local probes such as FTIR and RS that are complementary tools for XRD. Analysis was conducted using the spectroscopic D_{3d}^5 symmetry, but it is also convenient to analyze these vibrational spectra in terms of localized vibrations, considering the layered structures built of CoO_6 and LiO_6 octahedra. IR and Raman active modes correspond to vibrations involving primarily atomic motion of cations against their oxygen neighbors [(36)]. $LiCoO_2$ oxide with layered structure and crystallographic $R\bar{3}m$ space group has a corresponding spectroscopic space group of D_{3d}^5. As a general rule of the factor group analysis, the two Raman-active modes for $LiMO_2$ are located in the range 400–650cm^{-1} and the four infrared-active bands are observed in two distinct regions: the low-wavenumber infrared peak appears in the region 200–300cm^{-1}, whereas the

second group of three bands, *i.e.* the components of the rock-salt band, are recorded in the high-frequency region between 400 and 600cm^{-1} [37].

The RS and FTIR spectra of $LiCoO_2$ are shown in Fig.8 and 9.The two predicted E_g and A_{1g} Raman-active modes for $LiCoO_2$ are in good agreement with the factor group analysis of the $R\bar{3}m$ symmetry. They are located at 484 and 594cm^{-1}, respectively, which coincidence with the wavenumbers 485 and 595cm^{-1} for $LiCoO_2$[37]. The Raman bands are likely lie to the motions involving mainly the Co–O stretching and O–Co–O bending, as the contributions to the Raman modes are only from the motion of oxygen atoms. The A_{1g} mode has the greater oscillator strength and exhibits an intensity twice that the E_g mode.

The FTIR spectrum of $LiCoO_2$ displays features as follows. (i) The region of strong absorption corresponds to the broad rock-salt band, which is broken into several distinct components at 600, 556 and 498cm^{-1}, with a shoulder located at 643cm^{-1}. (ii) An isolated moderately sharp band at 267cm^{-1}. It is clear that IR bands of $LiCoO_2$ are broader than those in the Raman spectrum. As far as this band is concerned, isotopic ^{6}Li–^{7}Li replacement in $LiMO_2$ with the D^5_{3d} space group demonstrates that the far-infrared peak between 200 and 300 cm^{-1} is related to the vibration of an isolated LiO_6 octahedron. Thus, the band at 267cm^{-1}can be assigned with confidence to an asymmetric stretching vibration of LiO_6[37]. However, a small mixing of Li–O stretching and O–Co–O bending motion is present in the low-wavenumber peak.

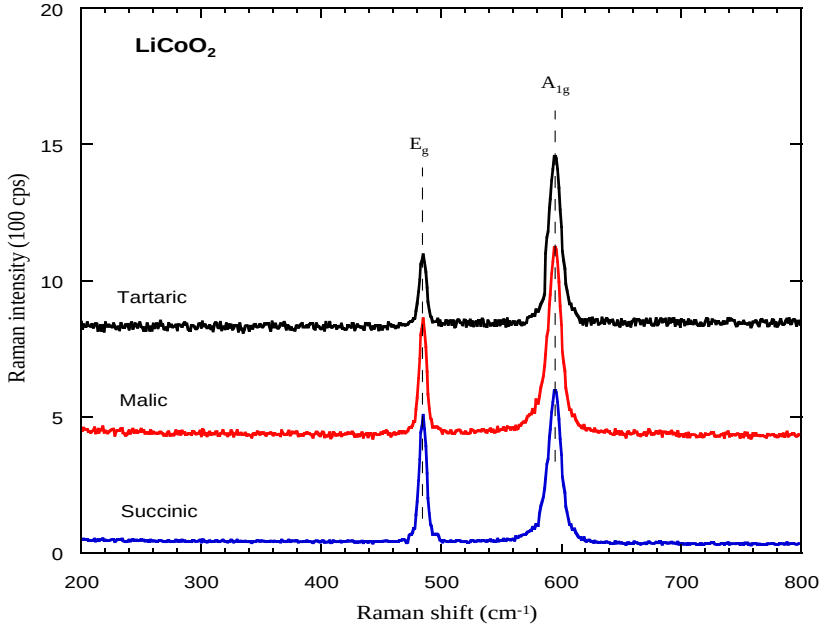

Fig. 8. Raman spectra of $LiCoO_2$ oxide synthesized at 800°C prepared by wet chemistry method, assisted by succinic, malic and tartaric acid.

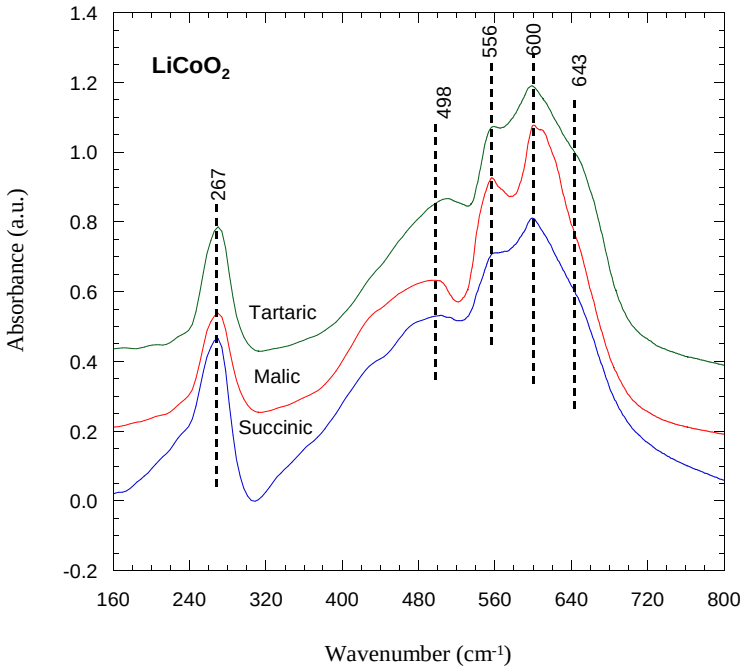

Fig. 9. FTIR absorption spectra of $LiCoO_2$ as a function of the of the chelating agents succinic, malic and tartaric acid, calcined at 800°C.

Study of the delithiated phase

Crystal structure

Structural properties have been investigated on chemically delithiated Li_xCoO_2 prepared in presence of the malic acid, selected for its better structural properties. The *x* (Li) was verified by XRD measurements. The XRD pattern of Li_xCoO_2 for $x \approx 0.3$ is shown in Fig.10, together with that of $x = 1$ sample for comparison. The XRD diagram of delithiated Li_xCoO_2 shows clearly that the (003) peak disappears with Li deintercalation and a new peak reappears (111), this feature indicates that the structural symmetry of Li_xCoO_2 (x=0.3) changed from hexagonal structure ($R\bar{3}m$; S.G) to spinel structure (*Fd3m*; S.G) upon Li deintercalation, this may be due to the chemical instability. The relative chemical stability and phase transition in the Li_xCoO_2 (x<<1) system can be understood by considering the electronic structure [38, 39] and the qualitative band diagram in Fig.11. For $LiCoO_2$ with a Co^{3+}:$3d^6$ configuration, the t_{2g} band is completely filled and the e_g band is empty. As lithium is extracted from $LiCoO_2$, the Co^{3+} ions are oxidized to Co^{4+}, which is accompanied by a removal of electrons from the t_{2g} band. Since the t_{2g} band overlaps significantly with the top of the O^{2-}:2p band, deeper lithium extraction with $x<0.5$ in Li_xCoO_2 may result in a removal of electrons from the O^{2-}:2p band as well. The removal of a significant amount of electrons from the O^{2-}:2p band will result in an oxidation of O^{2-} ions and an ultimate loss of oxygen from the lattice which leads to a phase transition.

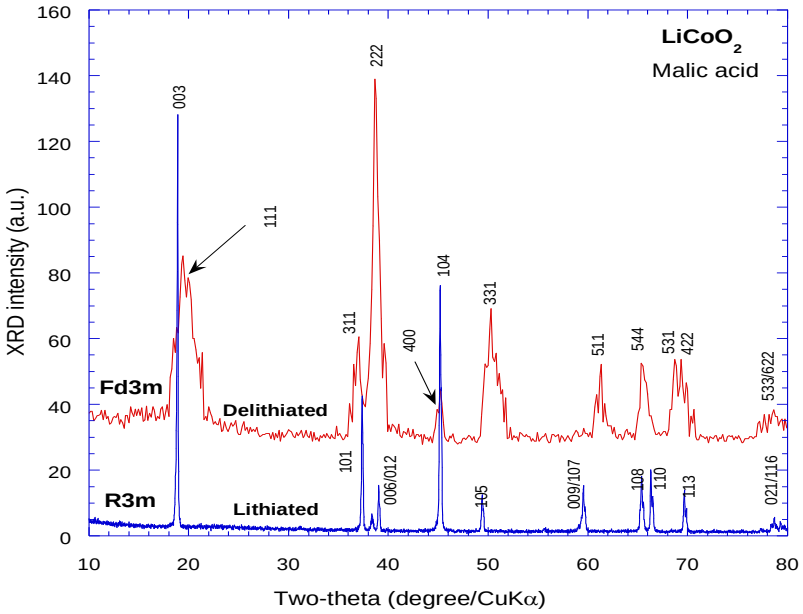

Fig.10. X-ray diffraction patterns for chemically deintercalated Li_xCoO_2 prepared samples.

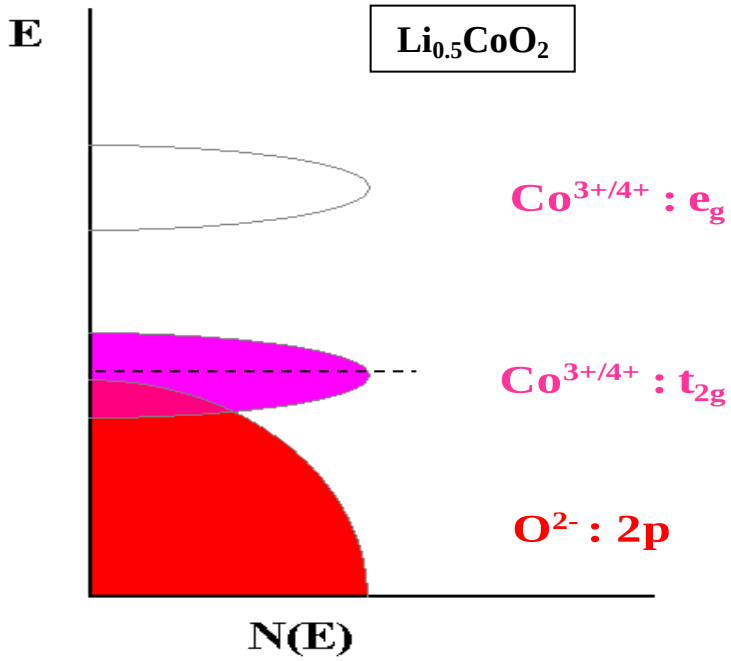

Fig.11. The band diagram of $Li_{0.5}CoO_2$.

Vibration spectroscopy

In order to understand the structure of $LiCoO_2$ samples in the charged state, the FTIR and RS spectra of chemically deintercalated Li_xCoO_2 (x<< 1) sample were studied. Fr+om the spectra shown in Fig. 12 and 13, it is clear that: (i) the frequency of LiO_6 octahedra is affected by lithium deintercalation, and (ii) displacement of the stretching peaks occurs. The frequency shift of LiO_6 vibrations implies that the octahedral oxygen environment of Li^+ ions is changed upon Li extraction. The strength of the LiO_6 peak decreases upon Li extraction due to the decrease of the density of oscillators. By calculating the area under this peak after and before delithiation we can deduce the amount of Li deintercalated from host materials during chemical delithiation process.

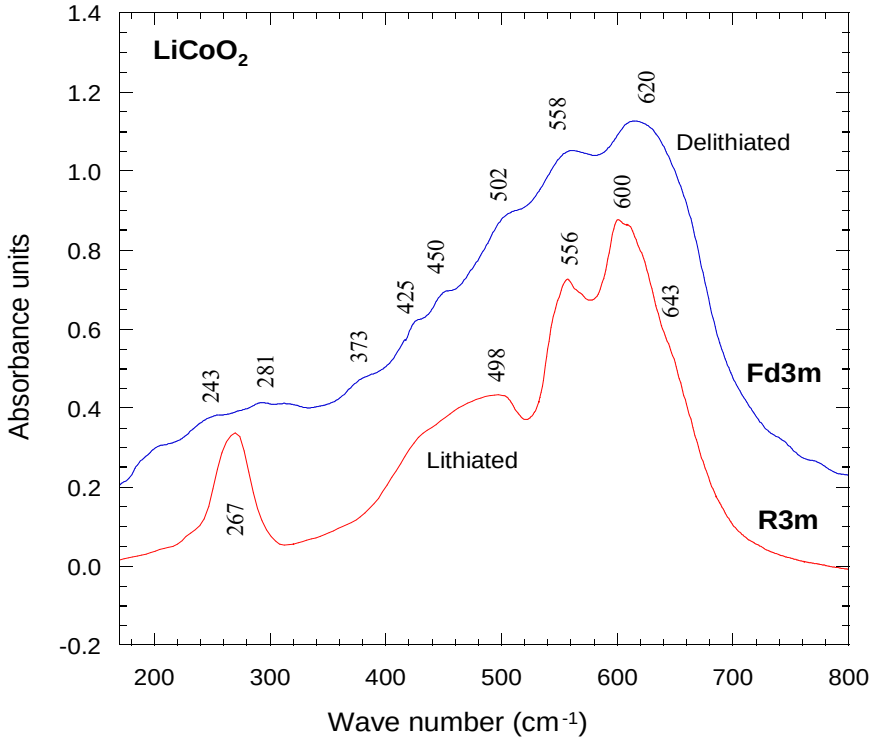

Fig. 12. FTIR spectra of the chemically deintercalated Li_xCoO_2 recorded at 25°C.

According to XRD data and factor group analysis, Fd3m spinel like structure has four vibrations infrared-active modes with $4F_{1u}$ species. All the IR bands belong to the F_{1u} species. The high frequency bands of the FTIR absorption spectrum of Li_xCoO_2 located approximately at 620 and 558cm^{-1}are attributed to the asymmetric stretching modes of MO_6 group, whereas the low-frequency bands at approximately 245, 281, 425,450 and 502cm^{-1} have a mixed character due to the presence of the bending modes of O-M-O bonds and modes of LiO_4

groups (Fig.12) [40]. The broadening of all the IR bands is associated with the disorder induced by the departure of Li ions. The broadening of the low frequency band is attributed to the random distribution of Li ions remaining in the host matrix.

Figure 13 shows the variation of the Raman spectra of delithiated $LiCoO_2$. Six Raman bands are observed as a result of decomposition with Gaussian profiles. We suggest that a delithiated $LiCoO_2$ sample adopts the spinel structural modification. We observe the formation of the modified-spinel structure without any impurity phases and the XRD patterns match based on Fd3m space group. Thus, the modified-spinel structure has a symmetry which contains similar modes, *i.e.* five modes are Raman active ($A_{1g}+E_g+3F_{2g}$). It is also convenient to analyze the vibrational spectra in terms of localized vibrations, considering the modified-spinel structure built out of MO_6 (M = Co) and LiO_6 octahedra [41]. The RS spectrum of Li_xCoO_2 is dominated by a strong and broad band at ca. 618cm^{-1} with two shoulders at 588 and 663 cm^{-1}. A band with medium intensity is recorded at 500 cm^{-1}, while weak bands are located at 663, 438, 375 and 318 cm^{-1}. Because the crystallographic anomaly does not affect the Raman spectrum either, we can definitely assume that the symmetry of the Li_xCoO_2 oxide belongs to Fd3m space group. The Raman band located at ca. 618cm^{-1} can be viewed as the symmetric O–M–O stretching vibration of MO_6 groups. This band is assigned to the A_{1g} symmetry in the O_h^7 spectroscopic space group. Its broadening may be related to the cation–anion bond lengths and polyhedral distortion occurring in Li_xCoO_2. The intensity of the shoulder located at 588cm^{-1} increase upon lithium deintercalation. The RS peak at 500 cm^{-1} has the E_g symmetry, whereas the peaks located at lower frequencies have the F_{2g} symmetry. The low-frequency mode at about 318cm^{-1}, labeled *LF*-mode, is unexpected mode always observed in this structure, which could be Raman active because of the cationic disorder that induced a breakdown on the transition symmetry [42]. This mode is tentatively related to the stretching mode of Li in octahedral coordination [43, 44]. As a result, a breakdown in the Raman and IR selection rules is expected, which explains the observation of broad bands (disorder) and the fact that more modes than expected are observed in the modified- spinel structure.

It can be stated that, in the modified-spinel Li_xCoO_2, the Co^{3+} and Co^{4+} cations are considered to be crystallographically equivalent (16d sites), in agreement with X-ray data; then, occupation probabilities of ½ must be affected for each cation in 16d. Hence, a loss of translation invariance certainly occurs, due to local lattice distortions around the different Co^{3+} and Co^{4+} cations. As a result, a breakdown in the Raman and IR selection rules is expected, which may explain the observation of broad bands (disorder) and the fact that more modes than expected are observed for the modified-spinel structure Li_xCoO_2.

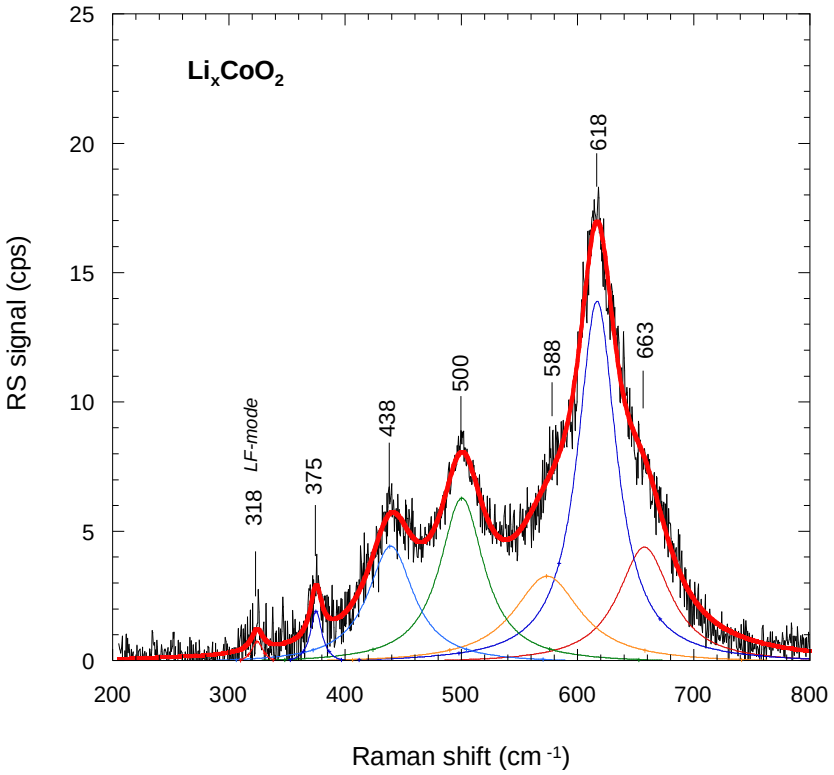

Fig.13. Raman spectrum of delithiated phase Li_xCoO_2. The thick solid lines correspond to the experimental data and fitted spectrum, the thin lines represent Gaussian line components of fitted spectrum.

Conclusion

In this paper, a sol-gel method was adopted to prepare nanometer $LiCoO_2$ using different complexing agent for lithium-ion batteries. $LiCoO_2$ powders were easily obtained with homogeneity, regular morphology, and narrow particle size distribution using wet chemistry method. The particle size of the $LiCoO_2$ powders increases with the increasing preparation temperature. The $LiCoO_2$ sample prepared at 800°C shows well crystallization with an ordered distribution of lithium and cobalt ions. Vibration spectroscopy is applied to compensate the limitation of XRD which cannot differentiate the crystal structure of the different phases of the $LiCoO_2$. Upon Li deintercalation, the structural symmetry of Li_xCoO_2 (x=0.3) changed from hexagonal structure ($R\bar{3}m$; S.G) to spinel structure (*Fd3m*; S.G), this may be due to the chemical instability.

References

1. **Chen, C.H., Hwang, B.J., Chen, C.Y., Hu, S.K., Chen, J.M., Sheu, H.S. and Lee, J.F.;** Soft X-ray absorption spectroscopy studies on the chemically delithiated commercial $LiCoO_2$ cathode material. *J. Power Sources*, **174**, 938 (2007).

2. **Chiang, Y.M., Jang, Y.I., Wang, H.F., Huang, B.Y., Sadoway, D.R., and Ye, P.X.;** Synthesis of $LiCoO_2$ by decomposition and intercalation of Hydroxides. *J. Electrochem. Soc.* **145**, 887 (1998).

3. **Ganguly, P., Venkatraman, T.N., Rajanohanan, P.R. and Ganapathy, S.,** Evidence for multiple M Sites in AMO_2 compounds: ^{59}Co solid state NMR studies on $LiCoO_2$. *J. Phys. Chem*. B, **101**, 11099 (1997).

4. **Kumta, P.N., Gallet, D., Waghray, A., Blomgren, G.E. and Setter, M.P.,** Synthesis of $LiCoO_2$ powders for lithium-ion batteries from precursors derived by rotary evaporation. *J. Power Sources***, 72**, 91 (1998).

5. **Tukmoto, H. and West, A.R.,** Electronic conductivity of $LiCoO_2$ and its enhancement by magnesium doping. *J. Electrochem. Soc.* **144,** 3164 (1997).

6. **Patrissi, C.J., and Martin, C.R.,** Sol-gel-based template synthesis and Li-insertion rate performance of nanostructured vanadium pentoxide. *J. Electrochem. Soc.* **146**, 3176 (1999).

7. **Shlyakhtin, O.A., Yoon, Y.S. and Oh, Y.J.,** Particle size control of $LiCoO_2$ powders by powder engineering methods. *J. Eur. Ceram. Soc*. **23**, 1893 (2003).

8. **Okubo, M., Hosono, E., Kim, J., Enomoto, M. Kojima, N., Kudo, T., Zhou, H.S. and Honma, I.,** Nanosize effect on high-rate Li-ion intercalation in $LiCoO_2$ electrode. *J. Am. Chem. Soc*. **129**, 7444 (2007).

9. **Jiao, F., Shaju, K.M. and Bruce, P.G.,** Synthesis of nanowire and mesoporous low-temperature $LiCoO_2$ by a post-templating reaction. *Angew. Chem. Int. Ed*. **44,** 6550 (2005).

10. **Afanasiev, P. and Geantet, C.,** Synthesis of solid materials in molten nitrates. *Coord. Chem. Rev*. **178**, 1725 (1998).

11. **Fu, J., Baia, Y., Liua, C., Yu, H. and Mo, Y.,** Physical characteristic study of $LiCoO_2$ prepared by molten salt synthesis method in 550–800°C. *Materials Chemistry and Physics* **115**, 105 (2009).

12. **Li, Y., Wan, C., Wu, Y., Jiang, C., Zhu, Y., and Power, J.,** Synthesis and characterization of ultrafine $LiCoO_2$ powders by a spray-drying method. *J. Power, Sources*, **85,** 294 (2000).

13. **Chen, H., Qiu, X., Zhu, W. and Hagenmuller, P.,** Synthesis and high rate properties of nanoparticled lithium cobalt oxides as the cathode material for lithium-ion battery. *Electrochem. Commun*. **4**, 488 (2002).

14. **Larcher, D., Palacin, M.R., Amatucci, G.G. and Tarascon, J.M.,** Electrochemically Active $LiCoO_2$ and $LiNiO_2$ made by cationic exchange under hydrothermal conditions. *J. Electrochem. Soc*. **144**, 408 (1997).

15. **Tabuchi, M., Ado, K., Kobayashi, H., Sakaebe, H., Kageyama, H., Masquelier, C., Yonemura, M., Hirano, A. and Kanno**, **R.,** Preparation of $LiCoO_2$ and $LiCo_{1-x}Fe_xO_2$ using hydrothermal reactions. *J. Mater. Chem*. **9**,199 (1999).

16. **Kobayashi, H., Shigemura, H., Tabuchi, M., Sakaebe, H., Ado, K., Kageyama, H., Hirano, A., Kanno, R., Wakita, M., Morimoto, S. and Nasu, S.,** Electrochemical properties of hydrothermally obtained $LiCo_{1-x}Fe_xO_2$ as a positive electrode material for rechargeable lithium batteries. *J. Electrochem. Soc*. **147**, 960 (2000).

17. **Burukhin, A., Brylev, O., Hany, P. and Churagulov, B.R.,** Hydrothermal synthesis of $LiCoO_2$ for lithium rechargeable batteries. *Solid State Ionics*, **151**, 259 (2002).

18. **Zhecheva, E., Stoyanova, R., Gorova, M., Alcantara, R. and Mopales, J.,** Lithium−cobalt citrate precursors in the preparation of intercalation electrode materials. *J.L. Tirado, Chem. Mater*. **8**, 1429 (1996).

19. **Peng, Z.S., Wan, C.R. and Jiang, C.Y.,** Synthesis by sol–gel process and characterization, of $LiCoO_2$ cathode materials. *J. Power Sources*, **72**, 215 (1998).

20. **Yoon, W.S. and Kim, K.B.,** Synthesis of $LiCoO_2$ using acrylic acid and its electrochemical, properties for Li secondary batteries. *J. Power Sources* **81**, 517 (1999).

21. **Yoshikawa, M., Mori, Y. Obata, H. and Maegawa, M.,** Raman scattering from nanometer-sized diamond. *J. Appl. Lett*. **67**, 694 (1995).

22. **Zi, J., Buscher, H., Falter, C., Ludwig, W., Zhang, K. and Xie, X.,** Raman shifts in Si nano-crystals. *J. Appl. Lett*. **69**, 200 (1996).

23. **Jia, T.J., Li, P.W., Shang, Z.G., Zhang, L. and Mo, Y.J.,** the study on raman and infrared spectra of furfural molecule. *J. Light Scattering*, **19**, 1 (2007).

24. **He, T.C., Jia, T.J., Du, Y.B. and Mo, Y.J.,** The study on surface-enhanced raman scattering of methyl orange. *J. Light Scattering*, **19**, 6 (2007).

25. **Du, Y.B., Cai, Z.P., He, T.C., Cheng, P.H., Jia, T. J. and Mo, Y.J.,** The SERS spectra of cds nanoparticles deposited in anodic aluminum oxide templates. *J. Light Scattering*, **19**, 206 (2007).

26. **Abdel-Ghany, A., Zaghib, K., Gendron, F., Mauger, A. and Julien. C.M.,** Structural, magnetic and electrochemical properties of $LiNi_{0.5}Mn_{0.5}O_2$ as positive electrode for Li-ion batteries. *Electrochimica Acta*, **52** 4092(2006).

27. **Julien, C., El-Farh, L., Rangan, S., and Massot, S.** Studies of $LiNi_{0.6}Co_{0.4}O_2$ cathode material prepared by the citric acid-assisted sol-gel method for lithium batteries. *J. Sol-Gel Sci*. & *Technol*. **15**, 63 (1999).

28. **Julien, C., Michael, M.S. and Ziolkiewicz, S.,** Synthesis and electrochemistry of $LiMn_2O_4$ prepared using succinic acid as complexing agent. *Int. J. Inorg. Mater.* **1**, 29 (1999).

29. **Julien, C.,** Structure, morphology and electrochemistry of doped lithium cobalt oxides. *Ionics* **6**, 30 (2000).

30. **Julien, C., El-Farh, L., Rangan, S. and Massot, M.,** studies of $lini_{0.6}co_{0.4}o_2$ cathode material prepared by the citric acid-assisted sol-gel method for lithium batteries. *J. Sol–Gel Sci. Technol.* **15**, 63 (1999).

31. **Julien, C., Ziolkiewicz, S., Lemal, M. and Massot, M.,** Synthesis, structure and electrochemistry of $LiMn_{2-y}Al_yO_4$ prepared by a wet-chemistry method. *J. Mater. Chem.* **11**, 1837 (2001).

32. **Garcia, S.C., Couceiro, A.C., Rodriguez, M.A.S., Soulette, F. and Julien, C.**, Influence of aluminum doping on the properties of $LiCoO_2$ and $LiNi_{0.5}Co_{0.5}O_2$ oxides. *Solid State Ionics*, **156**, 15 (2003).

33. **Lee, T., Cho, K., Oh, J. and Shin, D.,** Electrochemical characteristics of $LiCoO_2$ nano-powder synthesized via aerosol flame deposition (AFD). *J.Phys. Chem of Solids*, **69,** 1242 (2008).

34. **Vivekanandhan, S., Venkateswarlu, M. and Satyanarayana, N.,** Ammonium carboxylates assisted combustion process for the synthesis of nanocrystalline $LiCoO_2$ powders. *Materials Chemistry and Physics*, **109**, 241(2008).

35. **Clémencon, A., Appapillai, A.T., Kumar, S. and Shao-Horn, Y.,** Atomic force microscopy studies of surface and dimensional changes in Li_xCoO_2 crystals during lithium de-intercalation. *Electrochimica Acta* **52**, 4572 (2007).

36. **Julien, C. and Nazri, G.A.,** General overview of vibrational spectroscopy of layered transition-metal oxides. *Mater. Res. Soc. Symp. Proc.* **548**, 79 (1999).

37. **Julien, C.,** Local cationic environment in lithium nickel–cobalt oxides used as cathode materials for lithium batteries. *Solid State Ionics*, **136**, 887 (2000).

38. **Manthiram, A. and Choi, J.,** Chemical and structural instabilities of lithium ion battery cathodes, *J. Power Sources*, **159**, 249 (2006).

39. **Laubach, S., Schmidt, P. C., Ensling, D., Schmid, St., Jaegermann, W., Thissen, A., Nikolowski, K. and Ehrenberg**, **H.,** Changes in the crystal and electronic structure of $LiCoO_2$ and $LiNiO_2$ upon Li intercalation and de-intercalation. *Phys. Chem. Chem. Phys.* **11**, 3278 (2009).

40. **Julien, C.M. and Massot, M.,** Lattice vibrations of materials for lithium rechargeable batteries I. Lithium manganese oxide spinel. *Materials Science and Engineering*: **B 97,** 217 (2003).

41. **Nazri, G.A., Juliem, C., Rougier, A. and Poniato wski, E.H.,** Vibrational spectroscopy of lithium manganese spinel oxides *Mol. Cryst. Liq. Cryst.* **311**, 81(1998).

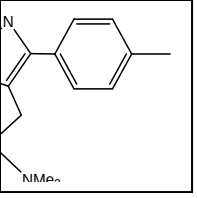

42. **Julien, C. M. and Massot, M. J.,** Raman spectroscopic studies of lithium manganates with spinel structure. *Phys. Condens. Matter*, **15,** 3151(2003).

43. **Julien, C., Letranchant, C., Lemal, M., Ziokiewicz, S., Castro S. and Garcia, J.,** Layered $LiNi_{1-y}Co_yO_2$ compounds synthesized by a glycine-assisted combustion method for lithium batteries. *J. Mater. Sci*. **37,** 367 (2002).

44. **Kopec, M., Dygas, J. R., Krok, F., Mauger, A., Gendron, F., Jaszczak-Figiel, B., Gagor, A., Zaghib, K. and Julien, C.,** Heavy-Fermion behavior and electrochemistry of $Li_{1.27}Mn_{1.73}O_4$. *Chem. Mater*. **21**, 2525 (2009).

(*Received* 16 /5/ 2010;
accepted 10 / 8 /2010*)*

التحضير و التوصيف التركيبي لأكسيد الكوبلت المرتبط بالليثيوم ($LiCoO_2$) و المنزوع منه الليثيوم باستخدام عوامل مخلبية مختلفة

اشرف السيد عبد الغني السيد، علي عيسي احمد عيد، عايدة عبد العا ل سالمان*، كارمن مصطفي شرابي *، و سوزان كمال عبد الحميد
قسم الكيمياء غير العضوية- المركز القومى للبحوث- الجيزة - و*قسم الكيمياء- كلية العلوم- جامعة الأزهر(فرع البنات) القاهرة- مصر.

تم تحضير أكسيد الليثيوم كوبالت$LiCoO_2$ ذوالتركيب الطبقى بطريقة السول جل؛باستخدام كلا من أحماض السكسينيك،الماليك والطرطريك كعوامل مخلبية. ولدراسة التركيب للأكسيد المحضربعد عملية خروج الليثيوم منه اى شحن البطارية فقد تم نزع الليثيوم كيميائيا باستخدام$K_2S_2O_8$ كعامل مؤكسد قوى . ولتوصيف هذه الأكاسيد المحضرة التى تحتوى على الليثيوم او عند خروجه منها كيميائيا تم استخدام التحليل الحرارى (TGA و DTA) ، حيود الأشعة السينية (XRD) ، الميكروسكوب الالكترونى الماسح (SEM) ، الميكروسكوب الالكترونى النافذ (TEM)، الأشعة فوق البنفسجية (FTIR) ، وأشعة رامان (RS) ، وبالتوصيف لطور الأكسيد المحتوى على الليثيوم والمنزوع منه اتضح لنا أن عينة الأكسيد المحضرة ذات تركيب طبقى من نوعية أكسيد ألفا فلورو الصوديوم وأظهرت العينات تماثلا فى شكل الحبيبات مع وجود تناسب بين الحجم ودرجة حرارة التحضيروتبين حدوث تغير فى الطور وظهور طور اخر جديد عند نزع الليثوم كيميائيا من العينة المحضرة باستخدام حمض الماليك.